World Academy of Science, Engineering and Technology
International Journal of Mathematical and Computational Sciences
Vol:3, No:5, 2009

Porous Particles Drying in a Vertical Upward Pneumatic Conveying Dryer

Samy M. El-Behery [1] , W. A. El-Askary [1,] K. A. Ibrahim [1] and Mofreh H. Hamed [2]

Abstract**—**A steady two-phase flow model has been developed to simulate the drying process of porous particle in a pneumatic conveying dryer. The model takes into account the momentum, heat and mass transfer between the continuous phase and the dispersed phase. A single particle model was employed to calculate the evaporation rate. In this model the pore structure is simplified to allow the dominant evaporation mechanism to be readily identified at all points within the duct. The predominant mechanism at any time depends upon the pressure, temperature and the diameter of pore from which evaporating is occurring. The model was validated against experimental studies of pneumatic transport at low and high speeds as well as pneumatic drying. The effects of operating conditions on the dryer parameters are studied numerically. The present results show that the drying rate is enhanced as the inlet gas temperature and the gas flow rate increase and as the solid mass flow rate deceases. The present results also demonstrate the necessity of measuring the inlet gas velocity or the solid concentration in any experimental analysis.

Keywords**—**Two-phase, gas-solid, pneumatic drying, pneumatic conveying, heat and mass transfer

I. Introduction

DRYING is an essential operation in the chemical, food, agricultural, ceramic, polymers and plastic, pulp and paper, pharmaceutical and wood processing industries.

One of the most widely used drying systems is the pneumatic dryer and is also known as flash dryer, which can be characterized as continuous-convective dryer. Pneumatic dryers are characterized by simultaneous momentum, heat and mass transfer processes between the dispersed material and the drying agent. The large surface area for heat and mass transfer result in higher drying rate and higher drying capacity. In these types of dryers the contact time between the drying medium and particulate material is relatively short (usually few seconds only). Therefore, these dryers are suitable for heat-sensitive materials and also for removing external moisture.

This allows higher inlet temperatures to be used than in many other dryers without unduly heating the product [1]. Pneumatic dryers are simple in construction and have low capital cost. Vertical type of construction, which facilitates installation in exiting buildings, is an advantage of pneumatic dryer systems [2].

The short residence time can, however, be a problem as an advantage. Small fluctuation in the feed rate can suddenly alter the heat and the mass balance along the tube and gives very different exit conditions. In order to solve the complexity of the process, many articles related to the theoretical and mathematical model have been published.

By employing a volumetric heat transfer concept, as used for rotary dryers, simple estimation procedures have been suggested by Perry and Chilton [3]. These procedures assumed that the particles were traveling at a steady velocity close to the gas velocity. Baeyens et al [1] pointed out that these methods can over-predict the required dryer length by 200% to 400%.

To model the acceleration zone accurately, a stepwise procedure has been suggested by many workers including Thorpe et al. [4], Kemp et al. [5] and Kemp and Oakley [6]. Although these procedures are considerable improvement on the steady-state, Kemp et al. [7] reported that they can still give errors of 50-100% in the tube length prediction. Baeyens et al. [1] and Radford [8] neglected the effect of acceleration zone near the feed point in their stepwise procedure.

A steady- state one-dimensional model for pneumatic drying of wet particle was presented by Levy and Borde [9]. They assumed a two-stage drying process, with mass transfer controlled by evaporation from a saturated outer particle surface in the first stage and by diffusion within the particle in the second stage. The model predictions were compared with the experimental data obtained in large scale and pilot scale pneumatic dryers and a good agreement was obtained.

Skuratovsky et al. [10-11] developed a two-dimensional steady-state model based on the two-fluid theory. The predictions of the model were compared to the same experimental data used by Levy and Borde [9]. The predictions of the two-dimensional model did not present any significant difference as compared to those provided by Levy and Borde [9]. However, the radial distribution of gas and solid velocities and moisture content results in uneven cross sectional, which may be an important aspect to be considered in drying processes.

Pelegrina and Crapiste [12] presented a one-dimensional model for drying of food particles. The model took into account the particle shrinkage during the drying process and the non spherical shape of the particle was considered in drag

[1] Faculty of Engineering, Menoufiya University, Shebin El-kom, Egypt, s_elbehery@yahoo.com
[2] Faculty of Engineering, Kafrelsheikh University, Kafrelsheikh, Egypt, mofrehhh@yahoo.com

and heat transfer coefficients. They assumed that the internal resistance does not control the mass and energy transfer between solid particles and air. They found that, in the low range of air flow rates; the pressure drop under drying conditions is higher than that under transport conditions. An opposite effect was observed at higher velocities. However, the model was not verified with experimental results.

Narimatsu et al. [13] investigated numerically and experimentally the drying process of porous alumina and solid glass particles in a vertical dryer. The model was for one-dimensional incompressible flow and the internal resistance did not control the heat and mass transfer. Dry solids were used in heat transfer experiments, and the measurements of heat transfer coefficient indicted that the maximum value of heat transfer coefficient occurred at the velocity of minimum pressure drop. Furthermore, it was noticed that the morphology of particles (porous or non porous) did not influence in the air temperature profiles.

Fyhr and Rasmuson [14-15] presented a more complex model for a pneumatic dryer considering a distribution of particle sizes for steam drying of wood chips. The model includes a comprehensive two-dimensional model for single particle drying of single wood ship and one-dimensional plug flow was assumed. The irregular movement and the non spherical shape of the wood ships were accounted by measuring drag and heat transfer coefficients. To validate the model, measurements of the temperature and pressure profiles as well as the final moisture content were carried out, and the predictions agreed well with the experimental results.

Unlike the above studies, which were performed in a vertical upward pneumatic dryer, Alvarez et al. [16] have studied numerically and experimentally the drying process in a vertical downward pneumatic dryer. The model was for non shrinkage spherical particle and steady state one-dimensional flow. Some experimental works on the pneumatic dryer were given also,by [17-19].

The present paper concerns with a one-dimensional model for a pneumatic drying of porous particles. The model formulations are similar to that of Levy and Borde [9] but the present model allows for higher temperature. The mass transfer process was obtained by the comprehensive single particle model described by Radford [8]. The model of Levy and Borde [9] assumes that the drying process stops and particle break-up occurs if the saturation pressure inside the wet core is greater than the ambient pressure. The gas pressure in the pneumatic drying process is around atmospheric pressure, therefore, according to their assumption, particle break-up may be occurred if the temperature inside the wet core exceeds 100oC at any point within the duct. Also, it is important to notice that the difference between the present model and that of Radford [8] is that Radford's model assumes constant pressure along the duct and neglects the velocity difference between the two phases.

II. MATHEMATICAL MODELING

To formulate the suggested model, a quasi-one dimensional situation has been considered. The model is concerned with the two-phase flow of gas and particles through a vertical pipe. The model which was developed by Hamed [20] has been modified and used here based on the following assumptions:

- The flow is one-dimensional and steady.
- The particles are spherical in shape.
- The gas phase is mixture of water vapor and dry air.
- All particles interaction is ignored in the model. This implies that any mass, heat or momentum transfer between particles is insignificant to the transfer between individual particles and the gas stream.
- The model assumes that the solid will be conveyed as discrete particles and that heat and mass transfer occur from individual particles.

A. Governing Equations

Based on the above mentioned assumptions the governing equations for the gas and dispersed phases are derived according to the basic laws of fluid mechanics as follows:

- The mass balance equation for the gas phase may be written as:

$$\frac{d}{dx}(\alpha_g \rho_g u_g A) = S_{mass} \tag{1}$$

- The momentum equation for the gas phase can be expressed as:

$$\frac{d}{dx}(\alpha_g \rho_g u_g^2 A) = -A\frac{dP}{dx} - \alpha_g \rho_g gA - F_{wg} + S_{mom} + S_{mass} u_d \tag{2}$$

- The total energy equation for the gas phase can be written as:

$$\frac{d}{dx}\left[\alpha_g \rho_g u_g A\left(H_g + \frac{u_g^2}{2}\right)\right] = Q_{wall} - \alpha_g \rho_g u_g Ag + S_{mass}\left(H_{wv} + \frac{u_d^2}{2}\right) + S_{energy} \tag{3}$$

Where, S_{mass}, S_{mom} and S_{energy} are mass, momentum and energy coupling source terms, respectively.

- The equation of motion for a particle in a gas is given by:

$$\frac{du_d^2}{dx} = \frac{3\rho_g C_D}{2\rho_d d_p}\left(u_g - u_d\right)\left|u_g - u_d\right| - 2g\left(1 - \frac{\rho_g}{\rho_d}\right) - f_p \frac{u_d \left|u_d\right|}{d} \tag{4}$$

where, C_D is the drag coefficient and it is calculated as given in [21] as:

$$C_D = \frac{24}{\mathrm{Re}_p} \qquad \mathrm{Re}_p \le 1$$
$$= \frac{24}{\mathrm{Re}_p^{0.646}} \qquad 1 < \mathrm{Re}_p \le 400$$
$$= 0.5 \qquad 400 < \mathrm{Re}_p < 3\times 10^5$$

where, $\mathrm{Re}_p = \rho_g d_p \left| u_g - u_d \right| / \mu_g$ is the particle Reynolds number.

The equation for particle temperature, assuming the temperature is uniform throughout the particle can be written as:

$$u_d m_p C_{pd} \frac{dT_d}{dx} = \chi \pi d_p^2 h (T_g - T_d) - \overset{o}{m}_d H_{fg} \tag{5}$$

The residence time of the particles at the gas phase was calculated as given in [9] as:

$$\frac{dt_d}{dx} = \frac{1}{u_d} \tag{6}$$

B. Coupling between phases

An important concept in the analysis of two-phase gas-solid flows is to consider the mutual effect between the two phases. The mass transfer source term per unit length can be obtained by multiplying the evaporation rate from a single particle, $\overset{o}{m}_d$, by the total number of particles in the control volume [9]:

$$S_{mass} = N_p \overset{o}{m}_d A \tag{7}$$

The number of particles per unit volume, N_p, can be expressed as:

$$N_p = \frac{6\alpha_d}{\pi d_p^3} \tag{8}$$

The momentum coupling source term due to the reverse effect of particles can be written as [20]:

$$S_{mom} = -N_p A \frac{1}{2} C_D \frac{\pi d_p^2}{4} \rho_p x (u_g - u_d) \left| u_g - u_d \right| \tag{9}$$

The energy coupling source term for the total energy equation evolves convective heat transfer and the work due to particle drag (first and second terms on the right hand side, respectively) [20].

$$S_{energy} = -N_p A h \chi \pi d_p^2 (T_g - T_d) + S_{mom} u_d \tag{10}$$

C. Friction force

The friction force per unit length between the pipe wall and the gas phase was estimated by,

$$F_{wg} = \pi d_{pipe} \frac{f}{2} \rho_g (\alpha_g u_g)^2 \tag{11}$$

The friction factor, f, can be calculated from the well-known Blasius formula. In addition, the friction factor between particles and the wall of the pipe as in [22] is,

$$f_p = 1.0503 Fr_p^{-1.831} \tag{12}$$

Where, $Fr_p = u_d/(g d_p)^{0.5}$ is the particle Froude number.

D. Description of the particulate solids

The model used in the present study assumes that the solids will be modeled as true spheres with a vastly increased surface area to allow for the roughness and protuberance, while the pores were envisaged as cylindrical, running from the surface to the particle centre, as depicted in [8]. The particulate solid properties given in Table 1 need to be determined and the following parameters that describe the solid particles can be developed through these properties as follows:

The sphericity, χ, can be defined as the ratio between the true surface area and the spherical surface area as given in [8] as:

$$\chi = \frac{A_{so} \rho_{sa} d_p}{6} \tag{13}$$

The critical water content of solids, X_{cr}, can be estimated from the following equation;

$$X_{cr} = \rho_w \left(\frac{1}{\rho_{sa}} - \frac{1}{\rho_s} \right) \tag{14}$$

The density of the dispersed phase, which is composed from liquid water and solid material, can be expressed as;

$$\rho_d = \rho_{sa} (1 + X) \tag{15}$$

The diameters of pores are assumed to be normally distributed around a mean value of dm with standard deviation of σ. The following equations were developed to describe this model mathematically [8].

The diameters of pores are assumed to be normally distributed around a mean value of dm with standard deviation of σ. The following equations were developed to describe this model mathematically [8].

$$\beta = -\frac{8}{d_{\min} A_{pore}} \left(\frac{1}{\rho_{sa}} - \frac{1}{\rho_s} \right) + \left[\frac{64}{d_{\min}^2 A_{pore}^2} \left(\frac{1}{\rho_{sa}} - \frac{1}{\rho_s} \right)^2 + \frac{4}{d_{\min} A_{pore}} \left(\frac{1}{\rho_{sa}} - \frac{1}{\rho_s} \right) - 1 \right]^{0.5} \tag{16}$$

$$d_m = \frac{4}{A_{pore} \rho_{sa} (1 + \beta^2)} \left(1 - \frac{\rho_{sa}}{\rho_s} \right) \tag{17}$$

$$\sigma = \beta d_m \tag{18}$$

Excel 2003 is used to generate the size distribution using the built in function NORMSDIST. The obtained distribution, shown in Fig. 1, is then fed to the computer program.

TABLE I PROPERTIES OF THE PARTICULATE SOLID [8]

Property	Value for alumina
Average particle diameter, d_p	0.0001 m
Diameter of smallest pores in solid, d_{min}	7×10^{-9} m
External solid surface area, A_{so}	333 m^2/kg dry solids
Internal solid surface area, A_{pore}	6×10^4 m^2/kg dry solids
Density of solid material, ρ_s	3700 kg/m^3
Density of average particle, ρ_{sa}	1600 kg/m^3
Heat capacity of dry solid, C_{ps}, as function of temperature (K)	$6.954\text{-}0.2803T^{-0.25}$-$11.604T^{-0.15}$ kJ/kg.K

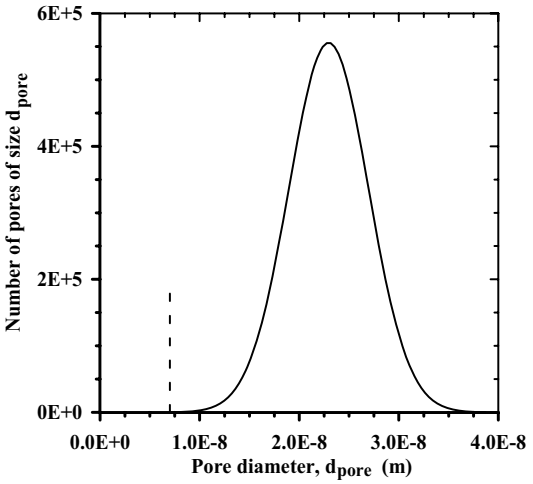

Fig. 1 Pore size distribution in an individual alumina particle

E. Heat transfer

The convective heat transfer coefficient, h, was calculated from Nusselt number, Nu, which is expressed as a function of Reynolds number, Re_p and Prandtl number, Pr, which are defined as:

$$Nu = \frac{hd_p}{\mu_g}; \qquad Pr = \frac{\mu_g C_{pg}}{k_g}$$

Various empirical correlations can be used to calculate the heat transfer coefficient. The following correlations have been tested in the present study:

- Frantz correlation [8]

The correlation was used by Radford [8] to calculate the heat transfer coefficient in pneumatic conveying dryer.

$$Nu = 0.015\, Re_p^{1.6}\, Pr^{0.667} \tag{19}$$

- De Brandt correlation [1, 9]

The correlation was developed for a pneumatic dryer.

$$Nu = 0.16\, Re_p^{1.3}\, Pr^{0.667} \tag{20}$$

- Debrand correlation [23]

The correlation was developed for a pneumatic dryer.

$$Nu = 0.035\, \mathrm{Re}_p^{1.15}\, \mathrm{Pr}^{0.333} \tag{21}$$

- Baeyens et al. correlation [1]

The correlation was developed for a large scale pneumatic dryer.

$$Nu = 0.15\, Re_p \tag{22}$$

- Modified Ranz-Marshall correlation [9]

The correlation was developed for single droplet/wet particle and it takes into account the resistance of the liquid vapor around the particle to the heat transfer by spalding number, B.

$$Nu = \frac{2 + 0.6\, Re_p^{0.5}\, Pr^{0.333}}{(1+B)^{0.7}} \tag{23}$$

$$B = \frac{C_{pwv}(T_g - T_p)}{H_{fg}} \tag{24}$$

- Modified Weber correlation [5]

An additional term proportional to $\mathrm{Re}_p^{0.8}$ was added to Ranz-Marshall correlation to account for turbulent flow.

$$Nu = 2 + \left(0.5\, Re_p^{0.5} + 0.06\, Re_p^{0.8}\right) Pr^{0.333} \tag{25}$$

The heat exchange per unit length between the surroundings and the gas phase, Q_{wall}, may be given as;

$$Q_{wall} = \pi d_{pipe} h_{pipe} (T_g - T_{wall}) \tag{26}$$

In the regime of well-developed turbulence, the relation between the coefficient of heat transfer between inner wall of the pipe and gas flow, h_{pipe}, and friction factor, f, can be expressed accurately with the dimensionless quantity as reported in [22] by;

$$\frac{h_{pipe}}{\rho_g u_g C_{pg}} = \frac{f}{2} \tag{27}$$

F. Mass transfer coefficient

In analogy to the heat transfer coefficient, h, the mass transfer coefficient, h_m, is calculated from Sherwood number, Sh, which is equivalent to Nusselt number, Nu. It is often expressed as a function of the particle Reynolds number, Re_p,

and Schmidt number, *Sc*, which equivalent to Prandtl number, *Pr*, and they defined as:

$$Sh = \frac{h_m d_p}{D_v}; \qquad Sc = \frac{\mu_g}{\rho_g D_v} \tag{28}$$

Eqs. 19-25 have been used to calculate the mass transfer coefficient in the present study.

G. Mass transfer rate

The mass transfer in the present model is based on the two-stage drying process. In the first stage, the solid surface can be considered to be fully wetted and the resistance to the mass transfer is located in the gas side. The evaporation rate from individual particle can be expressed as given in [9] as:

$$\overset{o}{m}_d = h_m \chi \pi d_p^2 \left(\frac{M_w p_{vo}}{\Re T_d} - \frac{M_w p_{vg}}{\Re T_g} \right) \tag{29}$$

Where, p_{vo} and p_{vg} are the partial pressures of water vapor at the particle surface and the gas phase.

The second drying stage period starts when the particulate surface becomes no longer wetted and evaporation must occur from within the pores. This was assumed to occur at solid water content, *X*, less than the critical solid water content, X_{cr}. Radford [8] mentioned that there are five possible mechanisms of evaporation during this period (the falling-rate period). The predominant mechanism at any time will depend upon the pressure, temperature and the diameter of pore from which evaporating is occurring. The five mechanisms are summarized blow.

Evaporation mechanism 1. It was mentioned earlier that the pores were envisaged as cylindrical, running from the surface to the particle centre. Evaporation from these pores will be aided by capillary action. The same surface tension effects that forced the water to the surface will lower the vapor pressure of the water, slowing its evaporation rate. The vapor pressure reduction is described by [8] as:

$$p_{vo1} = p_{vo} \exp\left(-\frac{4\sigma_t V_L}{d_{pore} R_g T_d} \right) \tag{30}$$

The surface tension force also produces a reduced pressure in the water immediately behind the meniscus (pressure reduction = $4\sigma_t/d_{pore}$) [8]. As the pore diameter decreases the pressure reduction increases and the pressure in the water decreases. If the pressure falls blow the vapor pressure at the prevailing temperature, the water behind the meniscus started to vaporize and the integrity of the meniscus will destroyed. In the pores with a small enough diameter for this to occur, a stable meniscus cannot form and the water contained in the pore will not be driven to the surface by the surface tension effects. The pore diameter at which the meniscus will break down, d_{men}, can be estimated from the following equation [8]:

$$d_{men} = \frac{4\sigma_t}{P - p_{vo}} \tag{31}$$

The water will evaporate from the hemispherical area at the pore end, and the evaporation rate from pores of diameter greater than d_{men} in an individual particle can be estimated from the following equation [8];

$$\overset{o}{m}_{d1} = \frac{h_m \chi \pi d_{pore}^2 N_{pore}}{2} \left(\frac{M_w p_{vo1}}{\Re T_d} - \frac{M_w p_{vg}}{\Re T_g} \right) \tag{32}$$

Where, N_{pore} is the number of pores of diameter d_{pore}.

Evaporation mechanism 2. In pores of diameter less than d_{men} the water will evaporate at a distance blow the surface. The vapor must find its way to the surface by either Fick or Knudsen diffusion flow. If the pore diameter is significantly greater than the mean free path of water molecules at the prevailing temperature and pressure, the vapor flow will be described by Fick diffusion. The evaporation rate from all bores of diameter greater than the free path of water vapor and less than d_{men} can be described as given in [24] by;

$$\overset{o}{m}_{d2} = \frac{18\pi d_{pore}^2 \chi N_{pore}}{4} \frac{D_v P}{R_g T_p \Delta Z} \frac{p_{vo} - p_{vg}}{p_{B,lm}} \tag{33}$$

Where, $P_{B,lm}$ is the log-mean pressure of non-H_2O gas and is given by;

$$p_{B,lm} = \frac{p_{vo} - p_{vg}}{\ln[(P - p_{vg})/(P - p_{vo})]} \tag{34}$$

The diffusion path length, ΔZ, can be estimated from Eq. (35) by assuming the pores are cylindrical of constant diameter through its entire length [8];

$$\Delta Z = \frac{d_p}{2} \frac{X_{cr} - X}{X_{cr}} \tag{35}$$

Evaporation mechanism 3. In pores of diameter comparable with the mean free path of water vapor molecules, the vapor flow is controlled by Knudsen diffusion rather than Fick diffusion. The rate of evaporation from all pores of diameter comparable with the mean free path of water vapor molecules in an individual particle will be given by [24]:

$$\overset{o}{m}_{d3} = 0.04433 \frac{N_{pore} \chi d_{pore}^3 (p_{vo} - p_{vg})}{\Delta Z (RT_d)^{0.5}} \tag{36}$$

The transition pore diameter from Fick diffusion to Knudsen diffusion was estimated by setting the evaporation rate by Fick diffusion equal to that by Knudsen diffusion as follows [8]:

$$d_{tran} = 1.612 \times 10^{-6} \frac{P T_d}{p_{B,lm} R^{0.5}} \tag{37}$$

Evaporation mechanism 4. In order to use either Fick diffusion or Knudsen diffusion, the value of the diffusion path length, ΔZ, must be defined. At a solid water content of X_{cr}, there will be no free water on the surface but all pores are totally. Therefore, ΔZ will be zero and Fick and Knudsen diffusions will yield infinite evaporation rate. As this an unrealistic situation, it was assumed that the evaporation from

the pores will initially be at the rate given by Eq. (32) but with reduced evaporation area (circular area instead of hemispherical area) and without the effect of surface tension on the vapor pressure [8]. Equation (32) can be rewritten to describe the current situation as follow:

$$\overset{o}{m}_{d4} = \frac{h_m \chi \pi d_{pore}^2 N_{pore}}{4}\left(\frac{M_w p_{vo}}{\Re T_d} - \frac{M_w p_{vg}}{\Re T_g}\right) \quad (38)$$

The evaporation rate form pores of diameter less than d_{men} will continue to be described by Eq. (38) until the value of evaporation rate given by Eq. (33) or Eq. (36) is less than that estimated by Eq. (38).

Evaporation mechanism 5. The equation for calculating the log-mean pressure of non-H_2O gas, $P_{B,lm}$, contains an implicit assumption that the vapor pressure at the surface from which evaporation is occurring, p_{vo}, is less than the total gas pressure, P. If the particle temperature is increased to a value at which the vapor pressure is greater than the total ambient pressure, then this assumption will be invalidated. At this condition, the evaporation rate will be controlled by the friction force. By assuming laminar flow of water vapor through the pores, the evaporation rate from pores of diameter d_{pore} will be given by [8];

$$\overset{o}{m}_{d5} = \frac{\pi \rho_{wv} d_{pore}^4 N_{pore} \chi}{128 \mu_{wv} \Delta Z}\left(p_{vo} - P\right) \quad (39)$$

The above five mechanisms describe the evaporation rate during the second drying stage (falling-rate period). The appropriate evaporation mechanism to any specific pore will depends upon the prevailing condition at the time under consideration. The selection of the drying mechanism must be established for each pore at the prevailing conditions. Therefore, this aspect will be discussed in a later section of this paper.

H. Supplementary Equations

In order to solve the above set of equations several supplementary equations, definitions and empirical correlations are required. These will be presented subsequently. It should be noted that both the gas and solid phases are mixtures and hence their thermodynamic properties are calculated using the mixture theory.

- The volume fraction equation

$$\alpha_g + \alpha_d = 1 \quad (40)$$

- Mass and mole fraction of water vapor in the gas stream

$$m_{wv} = \frac{\overset{o}{m}_{wv}}{\overset{o}{m}_{wv} + \overset{o}{m}_{da}};\ y_{H_2O} = \frac{m_{wv} M_{da}}{m_{wv} M_{da} + \left(1 - m_{wv}\right) M_{H2O}} \quad (41)$$

Where, M_{da} and M_{H_2O} are molecular weight of dry air and water vapor, respectively.

- Density of gas stream

The mole fraction of water vapor is used together with the ideal gas equation to calculate the density of the gas phase as follow:

$$\rho_g = P / R_g T_g \quad (42)$$

Where,

$$R_g = \Re / M_g;\ M_g = y_{H_2o} M_{H_2o} + \left(1 - y_{H_2o}\right) M_{da} \quad (43)$$

- Heat capacity of the gas stream

$$C_{pg} = m_{wv} C_{pwv} + \left(1 - m_{wv}\right) C_{pda} \quad (44)$$

- Viscosity of gas stream

$$\mu_g = y_{H_2O} \mu_{wv} + \left(1 - y_{H_2O}\right) \mu_{da} \quad (45)$$

- Thermal conductivity of gas stream

$$k_g = m_{wv} k_{wv} + \left(1 - m_{wv}\right) k_{da} \quad (46)$$

- Heat capacity of the dispersed phase

$$C_{pd} = \frac{X}{1+X} C_{pw} + \frac{1}{1+X} C_{ps} \quad (47)$$

The effect of temperature on the physical properties of water vapor and dry air is calculated from formula given in [25].

III. NUMERICAL METHOD

The system of equations (1-6) with the help of auxiliary and supplementary equations is solved numerically using the conservative variable formulation for the gas phase [26] and the fourth order Rounge-Kutta method is used for the dispersed phase. The conservative variable formulation is a cell by cell iterative procedure in which the gas phase variables are specified at the cell inlet and that at the cell exit are sought. The average values of the gas phase variables are then used to calculate the solid phase velocity and temperature. The source terms are then evaluated and new flow variables at the cell exit can be calculated. The procedure is continued until the gas velocity no longer changes with continued iteration. Once the solution is obtained for one cell, the exit conditions are taken as the starting condition for the adjacent cell and the procedure is repeated. More details about the application of conservative variable formulation for single phase and two-phase flows can be found in [26].

The mass transfer mechanisms obviously explained can be used to determine the evaporation from free surface water through the evaporation from the smallest pores in the porous particles. The evaporation rate from individual particle must be calculated for each iteration of the conservative variable formulation procedure. During the falling-rate period, the evaporation rate mechanisms cannot be distributed absolutely and must be established for each pore diameter under each set of conditions existing at the current iteration. Figure 2 depicts this aspect as it considered in the present model.

IV. MODEL VALIDATION

The present model was firstly validated against pneumatic transport data (without heat or mass transfer). Hariu and Molstad [27] measured the pressure drop in a vertical glass tube as a function of the solid mass flow rate. The same vertical tube, the same solid particles and the same initial

conditions are used to simulate the pressure drop in the present study. In the present model as well as Arastoopour and Gidaspow model [28], the initial void fraction or the initial solid velocity is needed. Because these values were not measured by Hariu and Molstad [27], the inlet gas void fraction was assumed to be 0.955 in both simulations. Figure 3 presents the comparison between the present predictions, the measured pressure drop by Hariu and Molstad [27] and the numerical predictions of Arastoopour and Gidaspow [28]. The predicted pressure drop using the correlation of Konno and Saito, reported in [1], is also presented in the figure. The figure indicates that the present model predicts the linear dependence of pressure drop with solid mass flow rate very well compared with that of [28]. The correlation of Konno and Saito predicts the linear variation of pressure drop with solid mass flow rate but with higher values than the experimentally observed and presently predicted.

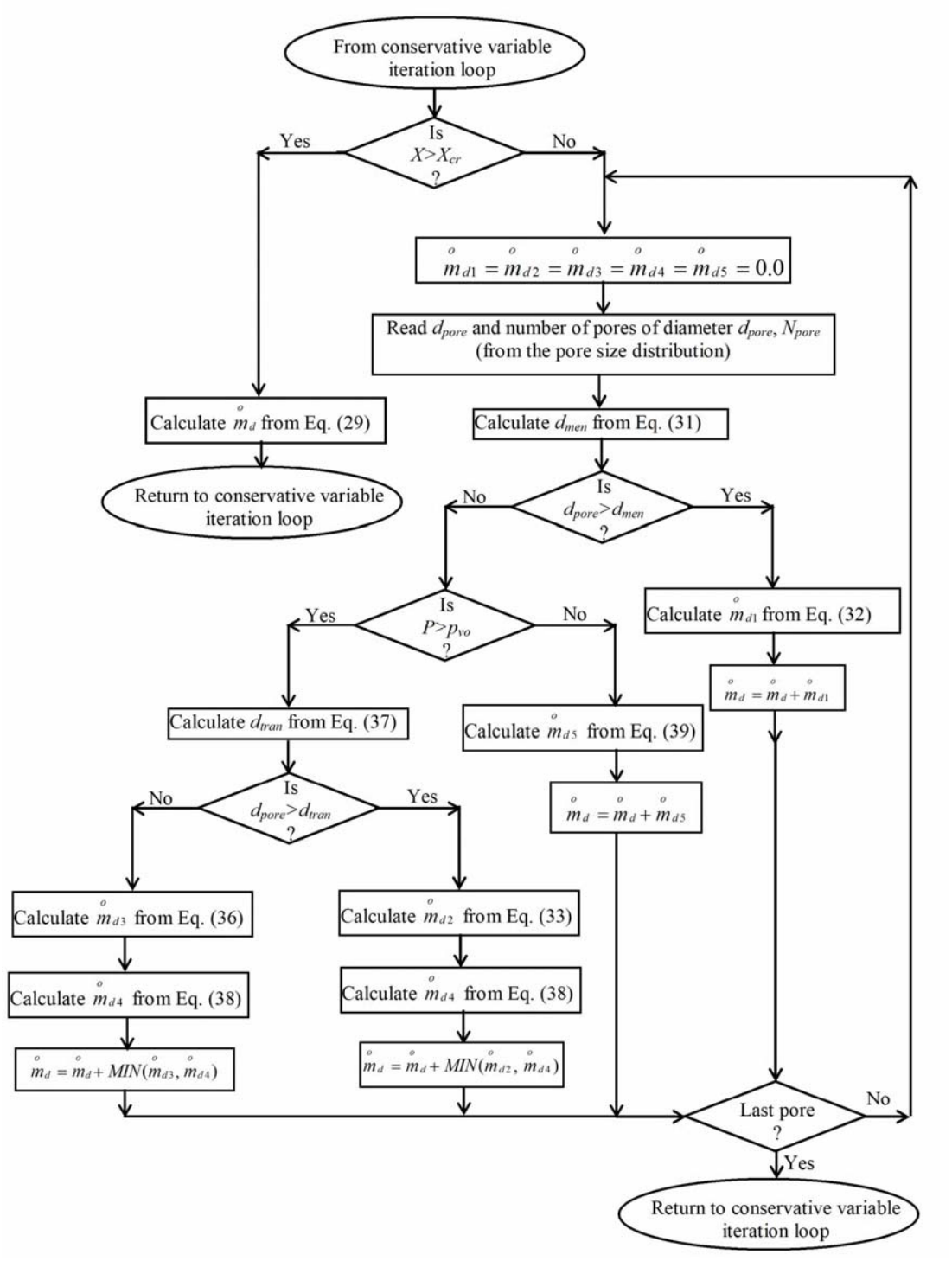

Fig. 2 A flowchart indicating distribution of evaporation mechanisms according to the prevailing conditions.

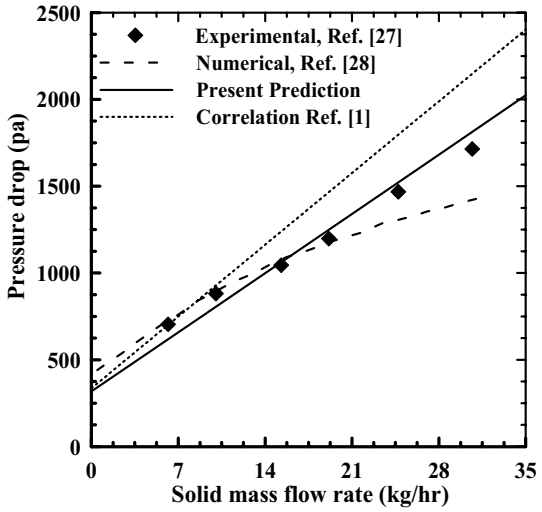

Fig. 3 Comparison between predicted pressure drop in a pneumatic conveying tube and published numerical and experimental results

For more validation of the present model, comparisons are carried out for high-speed gas-solid flow (choked flow). Mobbs et al. [29] measured the solid velocity for three types of solid particles in a brass pipe of ⅞ in (0.022 m) diameter and 148 ft (45.11 m) long. The conditions for the comparison are given in Table 2. Because the particles used in the experiment have a range of size, simulations are carried out for the largest and the smallest particles. Figure 4 shows the comparison between the present predictions and the measured solid velocity for the three types of solid particles. It can be seen from the figure that for the cases involving polystyrene-air suspension, the agreement between the computed and the measured values is reasonably good. The model under-predicts the solid velocity for the case involving silica-air suspension and over-predicts it for steel shot-air suspension. The irregularity of the silica particles has similar effect to the wall friction as it produces acceleration to the subsonic flow [20]. Since the drag coefficient and Nusslet number correlations used in the present model are for spherical particles, the model under-estimates the solid velocity, as shown in Fig. 4-b. The steel shot particles are heavier and the frequency of particle-wall collision is high. These are not taken into account in the present model. Therefore, the higher values of the predicted steel shot velocities are probably attributed to the absence of particle-wall collision in the present model. Overall, however, the agreement between the present model and the measured data for high-speed gas solid flow is quite acceptable.

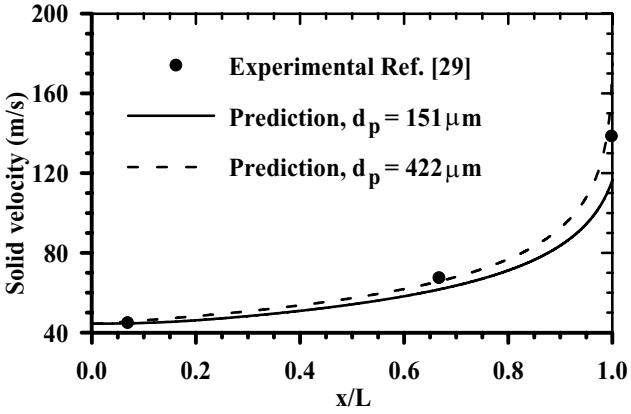

a. polystyrene

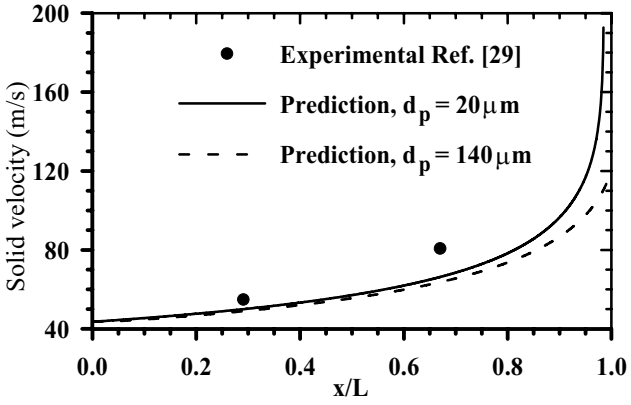

b. silica

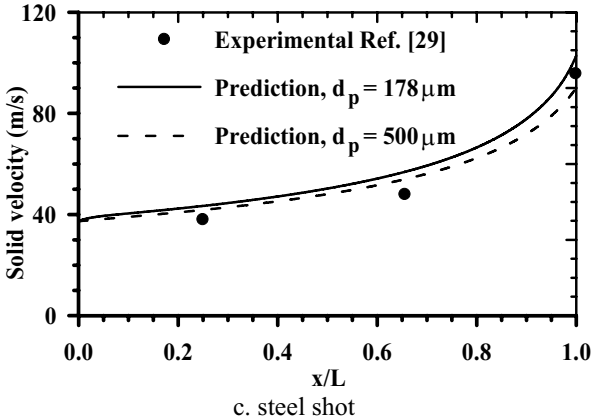

c. steel shot

Fig. 4 comparisons between predicted solid velocity and experimental data of Mobbs et al. [29]

TABLE II CONDITIONS FOR HIGH-SPEED GAS-SOLID FLOW COMPARISONS [29]

Type	ρ_d (kg/m^3)	d_p (μm)	$\dot{m}_g^o$ (kg/s)	$\dot{m}_s^o / \dot{m}_g^o$	C_{pd} (J/kg.K)
Polystyrene	1058	151-422	0.1040	2.328	1300
Silica	1200	20-140	0.1022	1.9458	703
Steal shot	7575	187-500	0.1153	1.6772	500

The model is then validated against pneumatic conveying dryer data. The experimental data of Radford [8] are selected for validation purpose. The conditions of the test cases are given in Table 3. The pipe diameter and length are 0.2 and 6 m, respectively. Because the inlet void fraction or the solid velocity is needed in the present model, the inlet solid velocity was assumed to be 0.2 of the inlet gas velocity.

Several Nusselt number correlations are tested in the present study. Figure 5 presents comparisons between the present predictions using different correlations and the experimental data given by previous investigations. It can be seen from the figure that the correlation of Baeyens et al. [1] gives the best agreement with experimental data. The outlet gas temperature and the outlet solid moisture content was under-predicted by about 4% and 0.6 %, respectively, when this correlation was applied. The modified Ranz-Marshall correlation [9] and the modified Weber correlation [5] are in acceptable agreement with the experimental data. They under-predict the outlet temperature and the outlet solid moisture content by about 5% and 20%, respectively. The figure shows also that the De Brandt correlation [1, 9] predicts the temperature profile fairly well while it over-predicts the solid moisture content by about 40%. On the other hand, Frantz [8] and Debrand [23] correlations give very poor results. Since the correlation of Baeyens et al. [1] gives the best predictions, this correlation is used in the present study to calculate the heat and mass transfer coefficients.

Figure 6 shows comparisons between the present predictions using Baeyens et al. correlation and the experimental results of Radford (1997) under different conditions. From this figure it can be seen that the present model predicts the gas temperature and solid water content very well. The figure shows also that the surface moisture is removed in the first few millimeters of the conveying duct. This can be attributed to the high inlet gas temperature and the high slip velocity between phases at this region.

TABLE III CONDITIONS FOR COMPARISON TEST CASES [8]

	Inlet gas temperature [k]	Inlet solid temperature [k]	Feed gas mass flow rate kg/sec	Wet solid mass flow rate	Water content of solid kg/kg dry solid	Water content in feed gas stream (%)
Case 1	873	300	0.5606	0.4897	0.41	3.5
Case 2	1073	300	0.4681	0.4767	0.41	4.5
Case 3	1173	300	0.5328	0.4990	0.41	4.8

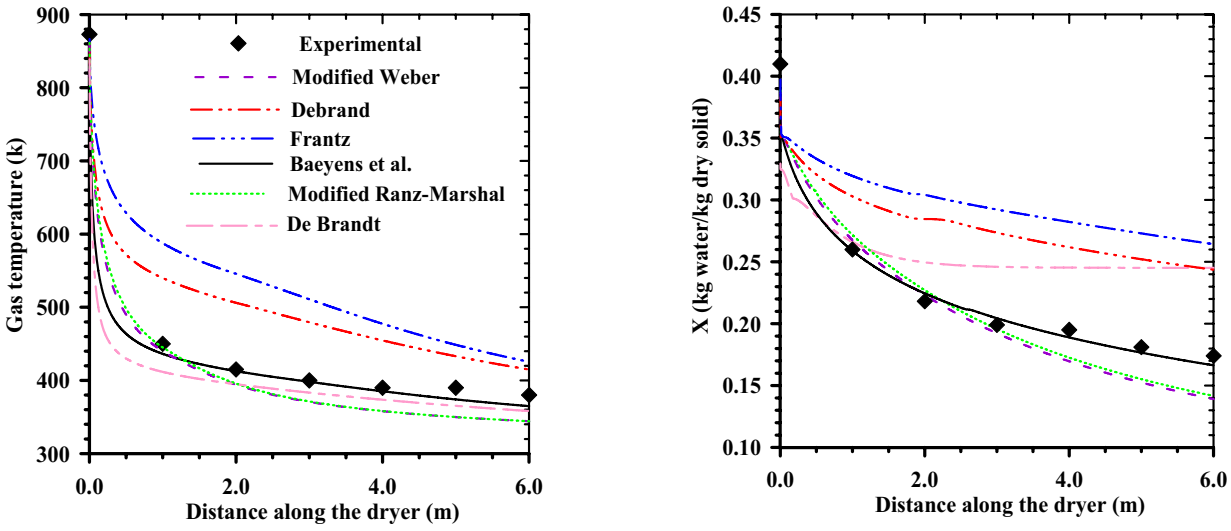

a- gas temperatures

b- water content

Fig. 5 Comparison between different heat and ass transfer correlations and experimental data (case 1)

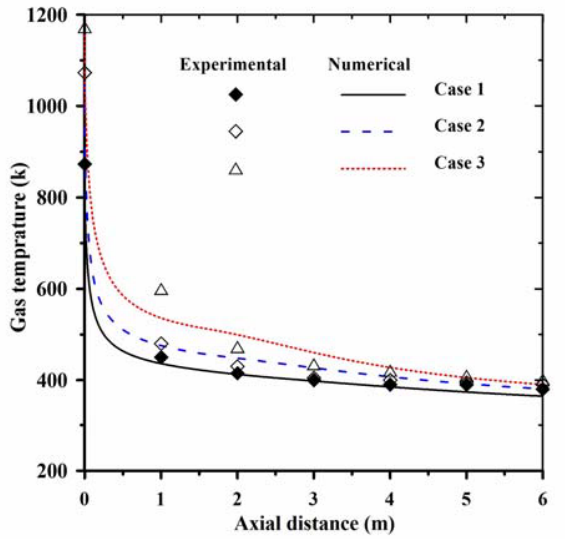

a- gas temperatures

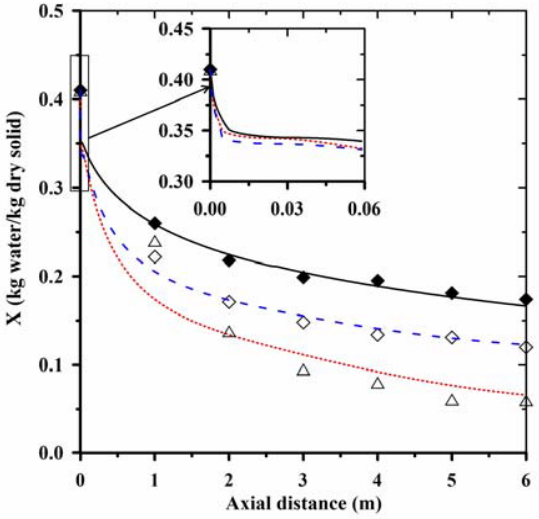

b- water content

Fig. 6 Comparison between present predictions and experimental results of Ref. [8].

V. Results and Discussion

The effects of inlet gas temperature, T_{gi}, air mass flow rate, $\overset{o}{m}_{air}$, solid mass flow rate, $\overset{o}{m}_{s}$ on the axial distribution of gas temperature, T_g, solid Temperature, T_d, gas velocity, u_g, solid velocity, u_d, solid water content, X, and gas water content, m_{H_2O} are studied for the parameters given in Table 4, as shown in Figs. 7-10. The same solid particles and the same pipe of Radford [8] are used in the simulations. In general, it can be seen from the figures that the gas temperature continuously decreases along the dryer, which in turn results in a decrease of the gas velocity. This can be attributed to the increase in gas density along the dryer with the decrease in gas temperature. The rapid decrease of gas temperature in the early stage of drying suggests that the pneumatic conveying dryer can be used for heat sensitive materials with higher inlet gas temperature. On entering the drying tube, the solid velocity increases rapidly then starts to decrease due to the decrease of gas velocity. Similar observations were reported by Kemp et al. [7]. The particles leave the dryer at a velocity approximately equal to that of the gas. The solid temperature firstly decreased in the few millimeters near the dryer inlet due to the high evaporation rate in this region and starts to increase after the free surface water is removed. Due to the continuous decrease of gas temperature, the solid temperature starts to decrease again. The maximum solid temperature occurs at a distance ranged between 0.25 and 1 m from the tube inlet, depending upon the inlet conditions.

TABLE IV SUMMARY OF PARAMETERS USED IN CALCULATIONS

Dry air mass flow rate (kg/s)	Dry solid mass flow rate (kg/s)	Inlet gas temperature (K)	Inlet velocity slip coefficient
0.45*	0.15	800*	0.1
0.75	0.35*	1000	0.2*
0.95	0.50	1200	0.3
* base case, X_i = 0.41 kg water/kg dry solid, T_{di} = 300 K , m_{wv} = 0.045 kg water vapor/kg dry air			

Figure 7 shows the effect of changing the inlet gas temperature with respect to the base case on the velocities, temperatures and moisture contents for both phases. It can be seen from this figure that the gas velocity increases as the inlet gas temperature increases. This is due to the decrease in gas density as the gas temperature increase. The figure also indicates that, as the gas temperature increases the solid temperature and the gas temperature content increase and the solid moisture content decreases. This is due to the fact that an increase in the gas inlet temperature results in an increase in the temperature difference driving force and the gas velocity, which in turn results in an increase in the heat and mass transfer coefficients.

The effect of drying air mass flow rate on the velocities, temperatures and moisture contents for both phases is presented in Fig. 8. It can be seen from this figure that as the air mass flow rate increases the gas velocity also increases. Two major phenomena take place as the superficial inlet gas velocity increases. The first, the particle residence time decreases with increasing superficial inlet gas velocity because particle velocity increases with increasing gas velocity, as shown in Fig. 8-b, and therefore the drying time reduces. The second, increasing gas velocity increases heat and mass transfer coefficient. Also, the total heat contained in the gas increases with increasing the gas mass flow rate at identical inlet gas temperature, so that the amount of heat provided to vaporize moisture in the particles increases as the gas mass flow rate. Both phenomena are working against each other depending on the characteristics of gas and particles as well as the hydrodynamic characteristics in the dryer. Namkung and Cho [18] and Bunyawanichakul et al. [30] reported that the drying rate increases as the inlet gas velocity increases while Pelegrina and Crapiste [12], Kaensup et al

[19] and Saravnan et al. [31] reported that the drying rate decreases as the inlet gas velocity increases. In the present study, the drying rate increases (the solid moisture content decreases) with increasing gas mass flow rate because the effect of increased heat and mass transfer on drying rate outweighs that of reduced particle residence time.

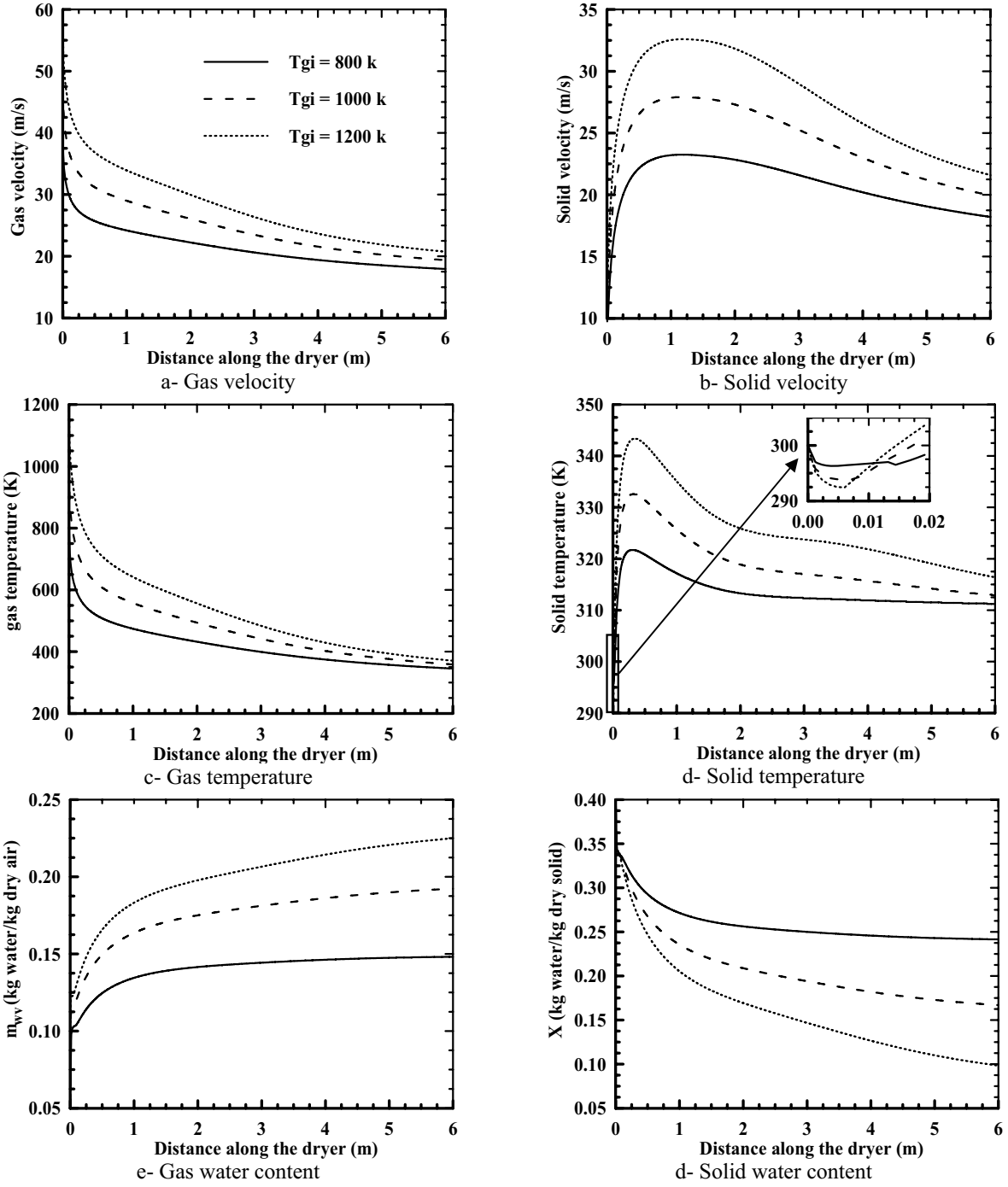

Fig. 7 Effect of inlet gas temperature, T_{gi}, on the axial distribution of velocities, temperatures and water content along the dryer for both phases

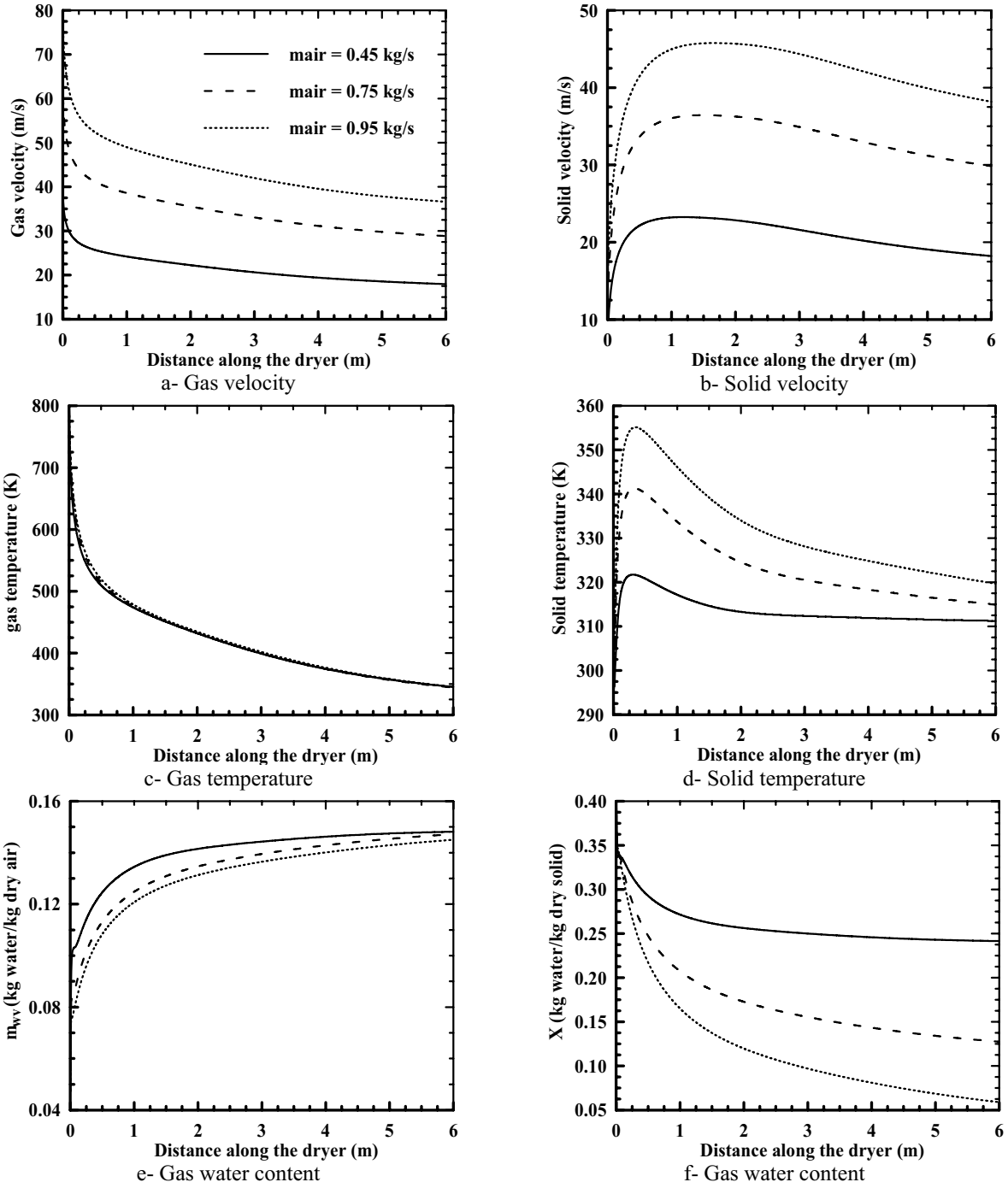

Fig. 8 Effect of air mass flow rate, $\dot{m}^{o}_{air}$, on the axial distribution of velocities, temperatures and water content along the dryer for both phases

Figure 9 presents the effect of solid mass flow rate on the velocities, temperatures and moisture contents for both phases. As the solid mass flow rate increases the solids holdup increases, resulting in an increased quantity of moisture in the system. This enhances the saturation of the drying gas, as shown in Fig. 9e, and decreases the gas temperature, as shown in Fig. 9c. As a result, the driving force for heat and mass transfer decreased, which eventually decreases the drying rate. Qualitative similar observations are reported by Saravanan et al. [31]. As the gas temperature decreases the gas density increases which in turn resulting in a decrease of both solid and gas velocities, as shown in Fig. 9a and b.

The present model as well as any other two-fluid model requires the definitions of the inlet parameters. The solids velocity or the solids void fraction is essential to calculate the gas phase void fraction and velocity by means of

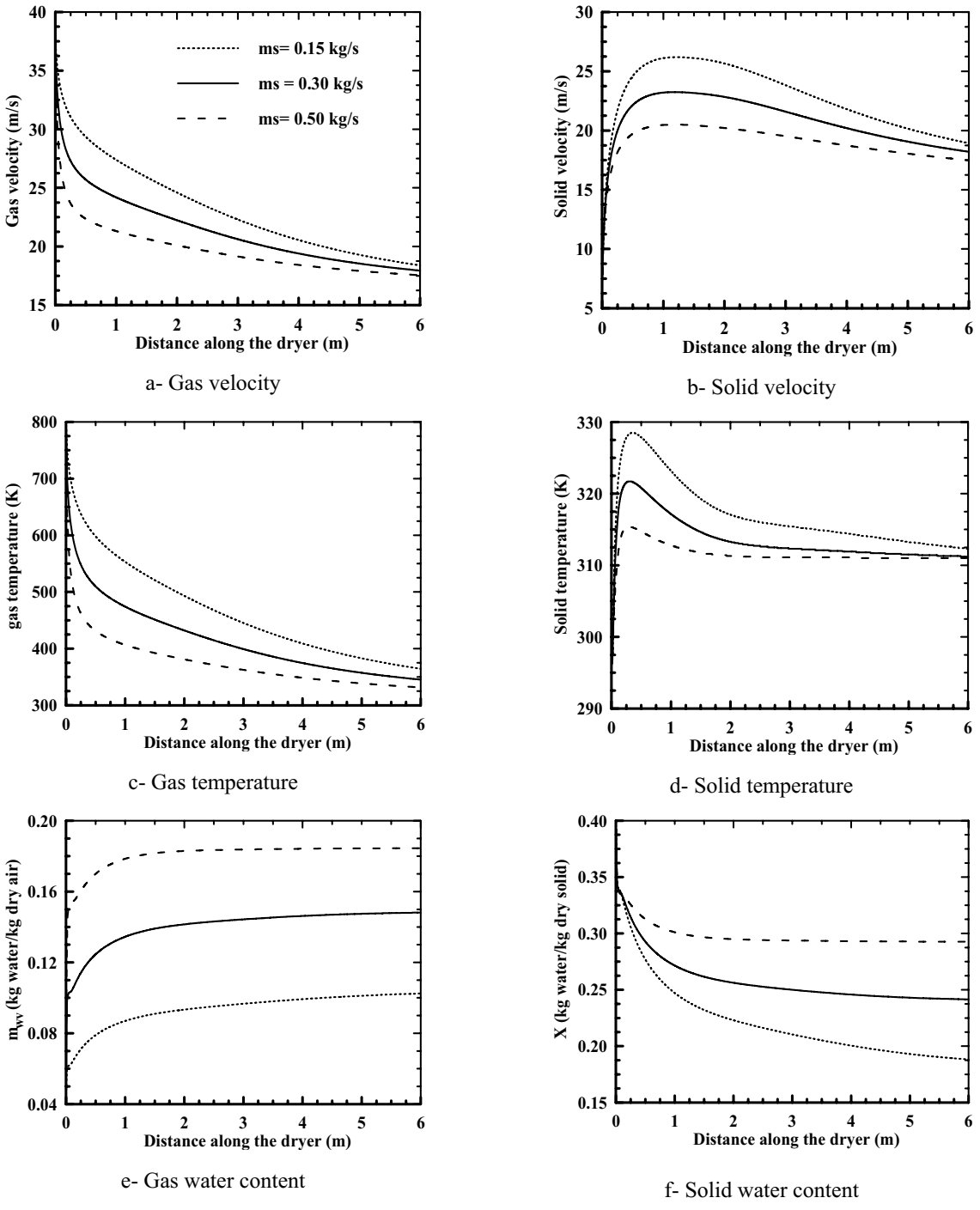

a- Gas velocity

b- Solid velocity

c- Gas temperature

d- Solid temperature

e- Gas water content

f- Solid water content

Fig. 9 Effect of solid mass flow rate, $\overset{o}{m}_s$, on the axial distribution of velocities, temperatures and water content along the dryer for both phases

void fraction equation, Eq. (40), and the gas phase continuity equation, respectively. The inlet solids velocity and the inlet solid void fraction are related by means of the solid phase continuity equation. However, these parameters are not usually measured. The effect of inlet slip coefficient, $S_{vo} = u_{di}/u_{gi}$, on the velocities, temperatures and moisture contents for both phases is presented in Fig. 10. It can be seen from this figure that the inlet solid velocity contributed in predicting the other properties of pneumatic conveying dryer. It also proves the necessity of measuring the void fraction or solid velocity in any experimental analysis.

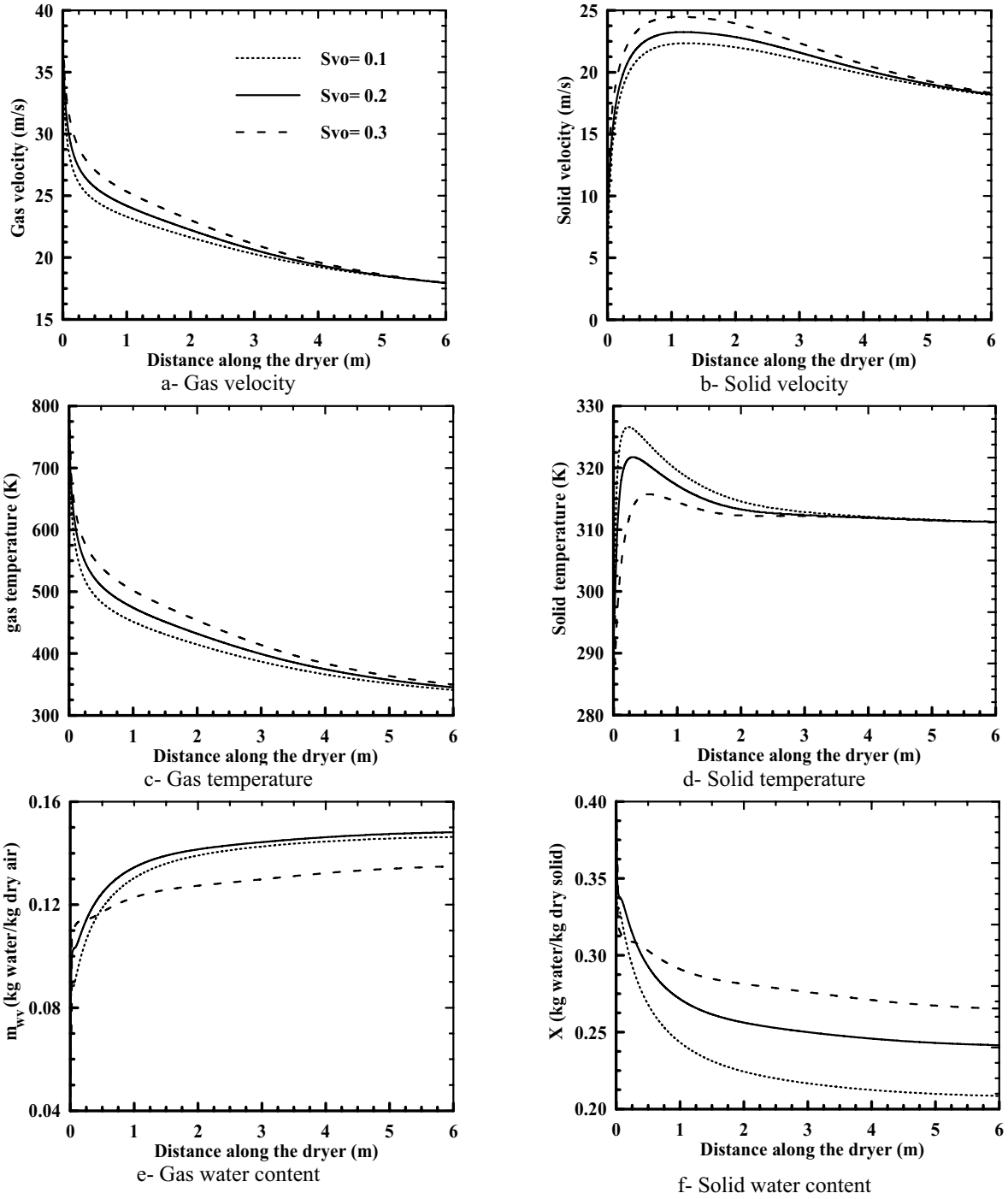

Fig. 10 Effect of inlet velocity slip coefficient, S_{vo}, on the axial distribution of velocities, temperatures and water content along the dryer for both phases.

VI. Conclusions

One-dimensional steady-state non-equilibrium two-phase model has been developed to demonstrate the drying of porous materials in a vertical upward gas-solid system. The model takes into account the momentum, heat and mass transfer between the continuous phase and the dispersed phase. The model was solved numerically using the conservative variables formulation for the gas phase and the fourth order Rounge-Kutta for the dispersed phase. The model was validated against pneumatic transport and pneumatic drying experimental results and a good agreement was obtained. The effects of different operating conditions on the properties of pneumatic drying were studied. It was found that the drying rate was increased as the inlet gas temperature or

the gas mass flow rate increased, while it was decreased as the solid mass flow rate was increased. Moreover, the model can be used to calculate the length of the drying tube for specific outlet solids moisture content.

NOMENCLATURE

A	Pipe cross-sectional area [m^2]
C_p	Specific heat [J/kg.K]
C_D	Drag coefficient [-]
d_{pipe}	Pipe diameter [m]
d_p	Particle diameter [m]
d_{pore}	Pore diameter [m]
D_v	diffusivity of water in air [m^2/s]
g	Gravity acceleration [m/s^2]
h	Heat transfer coefficient [$W/m^2.K$]
H	Enthalpy [J/kg]
H_{fg}	Latent heat of evaporation [J/kg]
h_m	mass transfer Coefficient [m/s]
k	Thermal conductivity [W/m.s]
m	Mass fraction [-]
M	Molecular weight [kg/kmol]
m_p	Mass of single wet particle [kg]
$\overset{o}{m}_d$	Evaporation rate from single particle [kg/s]
$\overset{o}{m}_{di}$	Evaporation rate by mechanism i [kg/s]
P	Total gas pressure [N/m^2]
P_{vg}	Partial pressure of water vapor in gas stream [N/m^2]
p_{vo}	water vapor pressure at T_d [N/m^2]
R	Gas constant [J/kg.K]
T	Temperature [K]
S_{v0}	Ratio between solid velocity and gas velocity (u_d/u_g)
t_d	Residence time [s]
u	Velocity [m/s]
V_L	Molar volume of water [m^3/kmol]
x	Axial distance along the dryer [m]
X	Solid phase moisture content [kg/kg dry solid]
y	Mole fraction [-]

GREEK LETTERS

α	Void fraction [-]
ρ	Density [kg/m^3]
μ	Viscosity [kg/m.s]
$\Re$	Universal gas constant [J/kmol.K]
σ	Standard deviation [m]
σ_t	Surface tension [N/m]
χ	Surface area shape factor (Sphericity)

Subscripts

cr	Critical
d	Dispersed phase
da	Dry air
g	Gas phase
H_2O	Water vapor
i	Inlet
s	Solid material
w	Water
wv	Water vapor

REFERENCES

[1] Baeyens J., Gauwbergen D. V. and Vinckier I., 1995, "Pneumatic Drying: the Use of Large-Scale Data in a Design Procedure", Powder Tech., Vol. 83, pp. 139-148.

[2] Borde I. and Levy A., 2006, "Pneumatic and Flash Drying", in Handbook of Industrial Drying, 3rd Ed., (Mujumdar A. S. Ed.), CRC Press, New York.

[3] Moyers C. G. and Baldwin G. W., 1997, "Psychrometry, Evaporative Cooling, and Solids Drying", in Perry's Chemical Engineers' Handbook, 7th Ed. (Eds. Robert H. Perry R. H., Green D. W. and Maloney J. O.), McGraw-Hill, Inc.

[4] Thorpe G.R., Wint A. and Coggan G.C., 1973, "The Mathematical Modelling of Industrial Pneumatic Driers", Transactions of the Institution of Chemical Engineers, Vol. 51, pp. 339–348.

[5] Kemp I. C., Bahu R. E. and Pasley H. S., 1994, "Model Development and Experimental Studies of Vertical Pneumatic Conveying Dryers", Drying Tech., Vol. 12, pp. 1323-1340.

[6] Kemp I. C and Oakley D. E., 1997, "Simulation and Scale-up of Pneumatic Conveying and Cascading Rotary Dryers", Drying Tech., Vol. 15, pp. 1699-1710.

[7] Kemp I. C., Oakley D. E. and Bahu R. E., 1991, "Computational Fluid Dynamics Modelling of Vertical Pneumatic Conveying Dryers", Powder Tech., Vol. 65, pp. 477-484.

[8] Radford R. D., 1997, "A Model of Particulate Drying in Pneumatic Conveying Systems", Powder Tech., Vol. 93, pp. 109-126.

[9] Levy A. and Borde I., 1999, "Steady State One Dimensional Flow Model for a Pneumatic Dryer", Chem. Eng. Processing, Vol. 38, pp. 121-130.

[10] Skuratovsky I., Levy A. and Borde I., 2003, "Two-Fluid Two-Dimensional Model for Pneumatic Drying", Drying Tech., Vol. 21, pp. 1645-1668.

[11] Skuratovsky I., Levy A. and Borde I., 2005, "Two-Dimensional Numerical Simulations of the Pneumatic Drying in Vertical pipes", Chem. Eng. Processing, Vol. 44, pp. 187-192.

[12] Pelegrina A. H. and Crapiste G. H., 2001, "Modelling the Pneumatic Drying of Food Particles", J. Food Eng., Vol. 48, pp. 301-310.

[13] Narimatsu C. P., Ferreira M. C. and Feire J. T., 2007, "Drying of Coarse Particles in a Vertical Pneumatic Conveyor", Drying Tech., Vol. 25, pp. 291-302.

[14] Fyhr C. and Rasmuson A., 1997, "Mathematical Model of Pneumatic Conveying Dryer", AICHE Journal, Vol. 43, pp. 2889-2902.

[15] Fyhr C. and Rasmuson A., 1997, "Steam Drying of Wood Ships in Pneumatic Conveying Dryers", Drying Tech., Vol. 15, pp. 1775-1785.

[16] Alvarez P. I., Vega R. and Blasco R., 2005, "Cocurrent Downflow Fluidized Bed Dryer: Experimental Equipment and Modeling", Drying Tech., Vol. 23, pp. 1435-1449.

[17] NamKung W. and Cho M., 2004, "Pneumatic Drying of Iron Ore particles in a Vertical tube", Drying Tech., Vol. 22, pp. 877-891.

[18] Kaensup W., Kulwong S. and Wongwises S., 2006, "A Small-Scale Pneumatic Conveying Dryer of Rough Rice", Drying Tech., Vol. 24, pp. 105-113.

[19] Kaensup W., Kulwong S. and Wongwises S., 2006, "Comparison of Drying Kinetics of Paddy Using a Pneumatic Dryer with and without a Cyclone", Drying Tech., Vol. 24, pp. 1039-1045.

[20] Hamed M. H., 2005," Choked Gas-Solid Two-Phase Flow in Pipes", J. Eng. Applied Science, Faculty of Engineering, Cairo University, Vol. 52, pp. 961-980.

[21] Kladas, D. D. and Deorgiou, D. P., 1993, "A Relative Examination of CD–Re Relationships used in Particle Trajectory Calculations", Trans. of ASME, J. of Fluids Engineering, Vol. 115, pp. 162-165.

[22] Han, T., A. Levy, and Y. Peng, 2000, "Model for Dilute Gas-Particle Flow in Constant-Area Lance with Heating and Friction ", Powder Technology, Vol. 112, pp. 283-288.

[23] Debrand S., 1974, "Heat Transfer during a Flash Drying Process", Ind. Eng. Chem., Process Des. Develop., Vol. 13, pp. 396-404.

[24] Welty J. R., Wicks G. E. and Wilson R. E., 1984, "Fundamentals of Momentum, Heat, and Mass Transfer", 3rd Ed., John Wiley & Sons, New York.
[25] Reynolds W. C., 1979, "Thermodynamic Properties in SI: Graphs, Tables and Computational Equations for Forty Substances", Published by the Department of Mechanical Engineering, Stanford University, Stanford CA 94305.
[26] Crowe C., Sommerfeld M. and Tsuji Y., 1998, "Multiphase Flow with Droplets and Particles", CRC Press, Florida, USA.
[27] Hariu O. H. and Molstad M. C., 194, "Pressure Drop in Vertical Tubes in Transport of Solids by Gases", Industrial and Engineering Chemistry, Vol. 41, pp. 1148-1160.
[28] Arastoopour H. and Gidaspow D., 1979, "Vertical Pneumatic Conveying Using Four Hydrodynamic Models", Ind. Eng. Chem. Fundam., Vol. 18, pp. 123-130.
[29] Mobbs F. R., Bowers H. M., D. M. Riches D. M., and Cole B. N., 1969-70, "Influence of Particle Size Distribution on the high-Speed flow of Gas-Solid Suspensions in a Pipe", Proc Instn Mech Engrs, Vol. 184, Pt 3C, paper 9.
[30] Bunyawanichakul P., Walker G. J., Sargison J. E. and Doe P. E., 2007, "Modelling and Simulation of Paddy Grain (Rice) Drying in a simple Pneumatic Dryer", Biosystems Eng., Vol. 96, pp. 335-344.
[31] Saravanan B., Balsubramaniam N. and Srinivasakannan C., 2007, "Drying Kinetics in a Vertical Gas-Solid System", Chem. Eng. Tech., Vol. 30, pp. 176-183.